X-646-72-241

PREPRINT

NASA TM X-65962

RING CURRENT PARTICLE DISTRIBUTIONS DURING THE MAGNETIC STORMS OF DECEMBER 16-18, 1971

P. H. SMITH

R. A. HOFFMAN

JULY 1972

GSFC

GODDARD SPACE FLIGHT CENTER

GREENBELT, MARYLAND

RING CURRENT PARTICLE DISTRIBUTIONS DURING THE MAGNETIC STORMS OF DECEMBER 16-18, 1971

By

P. H. Smith

and

R. A. Hoffman

NASA-Goddard Space Flight Center
Greenbelt, Maryland

JULY 1972

RING CURRENT PARTICLE DISTRIBUTIONS DURING THE MAGNETIC STORM OF DECEMBER 16-18, 1971

INTRODUCTION

Although previous measurements have been made on proton distributions in the ring current region, especially those by Frank (1967) of low energy protons from 200 eV to 50 keV and by Davis and Williamson (1966) of high energy protons with energies greater than 100 keV, S^3-A (Explorer 45) is providing the first total proton energy density measurements in the storm time ring current region. Detectors aboard S^3-A, which have been briefly described by Longanecker and Hoffman (1972), have yielded data on the proton energy density in the equatorial region of the earth's magnetosphere from L=2.5 R_E to L=5.5 R_E.

The results presented in this paper are derived from proton data taken during the geomagnetic storms of 16-18 December, 1971, which occurred approximately one month after the satellite was launched. Cahill (1972) has presented the magnetometer measurements from S^3-A and has also shown some ground magnetograms describing the magnetic field variations during these storms. Both storms initiated with a sudden commencement and positive phase, but the main phase of the first storm did not fully develop. This Letter will concentrate on the proton energy density distributions during the storms and contrast the development of the ring current for the two events.

DATA

The proton measurements on S^3-A are from three detector systems which collectively measure protons in the energy range 0.8 keV to 3800

keV. Subsets of these data used in this report are from the following detectors:

1. Channel Multiplier Proton Detector from which measurements from 5 to 30 keV are used;
2. Solid State Proton Detector, Low Energy mode, which measures 24 to 300 keV protons;
3. Solid State Proton Detector, High Energy mode, with measurements of 390 to 872 keV protons.

The orbital period of the spacecraft is approximately 7.8 hours with apogee during December 16-18, 1971, at 2100h magnetic-local-time. On an outbound leg L=3 was at 1800h and on the inbound leg L=3 was near midnight (Longanecker and Hoffman, 1972).

RESULTS

We have considered the relative contributions to the total energy density from the three energy regions, extrapolating from 300 to 390 keV in the third region, and find that the relative contributions are a function of altitude and magnetic storm conditions. Proton energy density radial profiles are first shown for three time periods: 1) immediately before the first sudden commencement, 2) in the growth phase after the first sudden commencement and 3) during the recovery phase of the second magnetic storm.

The proton energy density radial profiles at the magnetic equator are shown in Figure 1 for Orbit 98. The outbound portion of this orbit was during a magnetically quiet time which had followed a long period of quiet magnetic conditions. The sudden commencement of the first of the magnetic storms occurred when the S^3-A satellite was near apogee.

The inbound portion of this orbit was during the growth phase of the first storm which did not fully develop a main phase.

During this time period the energy density of the high energy protons in the range 300-872 keV contributed most substantially to the total energy density in the region 2.5 R_E to 4.0 R_E. It is important to note that the distributions for the outbound and inbound legs of the orbit for these high energy protons are quite symmetric even after the sudden commencement. High energy protons (> 100 keV) have been measured on other Explorer satellites, Explorers 12, 14, 15, and 26, (Davis and Williamson, 1966) and it is these protons which represent the quiet-time ring current (Sugiura, 1972).

A difference in radial profiles before and after the sudden commencement is most clearly seen in the 5-24 keV protons. There is a steep rise in the energy density shortly after apogee, (i.e., after the SC) which could quite well be a temporal effect associated with the growth of the storm.

The mid-energy protons in the range 24-300 keV provide most of the energy density above 4.5 R_E. A comparison between the outbound and inbound portion shows a slight enhancement from apogee to 4.5 R_E on the inbound leg, which is the same region in which the enhancement occurred for the low energy protons. The contribution to the increase comes from the low energy channels in this energy range.

The energy density radial profiles for Orbit 102 are shown in Figure 2 for the same three energy regions. This orbit was during the recovery portion of the second magnetic storm when the magnetic field at the surface of the earth was depressed by about 65γ.

The high energy protons by this time had been significantly depleted and only contributed 10% to the total proton energy density at L=3, or 2.7×10^{-8} ergs/cm^3. The mid-energy protons contributed the major amount to the energy density but both the mid- and low-energy protons were enhanced over the quiet-time period.

The energy density profiles for the inbound and outbound legs for all three energy regions are quite symmetric, which indicates that the ring current was also symmetric. The maximum in the total energy density radial distribution of 3×10^{-7} ergs/cm^3 was an increase of 300% over the quiet time period, while in the region 4.0 - 5.5 R_E the increase was over 100%.

During this December, 1971, period the maximum total energy density for the 5 to 872 keV protons occurred during the main phase of the second magnetic storm at L=4 on the outbound leg of Orbit 101 where it reached 5.5×10^{-7} ergs/cm^3. Figure 3 shows that the differential energy density spectrum (ergs/cm^3-keV) at this time had a broad maximum at about 40 keV, whereas, in contrast, the quiet-time spectrum of Orbit 97 taken at the same L-value and magnetic local time showed relative maximums at 10 keV and 200 keV with a minimum at about 50 keV. Thus the storm-time ring current constitutes an enormous enhancement of protons in the energy range 10 to 120 keV.

The high energy end of the spectrum from Orbit 101 shows the decrease from the quiet spectrum, but both spectrums between 300 and 530 keV require some shifts in the effective energy windows for the lower

energy channels in the high energy mode of the detector due to the steep energy spectrums. Such corrections, which have not been made, will decrease the differential energy densities in this energy range, thus making the spectrums above and below 300 keV match very well.

STORM DEVELOPMENT

To contrast the development of the ring current for the two storms, we now consider those protons (5 to 138 keV protons were used) which contribute substantially to the storm-time ring current. While protons in this energy regime contribute only 20% or less to the total energy density during magnetically quiet periods, their enhancement during magnetic storms combined with a depletion of protons with energies greater than about 170 keV make them the dominant (greater than 90%) contributors to the storm time densities (see Figure 3).

Figure 4 shows the energy density in the equatorial region as a function of L for these protons for four orbits associated with the first magnetic storm. The first orbit, 97, represents the quiet-time configuration, with a maximum energy density slightly over 2×10^{-8} ergs/cm^3 near apogee.

Orbit 98, which was discussed before, contrasts this quiet period represented by the outbound leg to the disturbed period represented by the inbound leg of this orbit. The enhancement in Orbit 98 over the quiet-time level of Orbit 97 corresponds in time to the magnetic variations in both the high and low latitude magnetograms shown by Cahill (1972).

Orbit 99 has a sharp rise near L=4.3 in the outbound leg and continues at a rather high level of intensity through apogee and down to an L of 3.2. In the next orbit, Orbit 100, the sharp rise occurs closer in, near L=3.6, and remains at a relatively high level through apogee. However, on the inbound leg a radial gradient of a similar nature to the previous orbit (and as will be seen, for the following three orbits) is not observed. This decrease in intensity appears to be caused by a loss of particles down the field lines rather than a retraction of the storm-time ring current to greater distances, for the latter would produce a gradient as steep or steeper than Orbit 99 due to the inward motion of the satellite. Note that the region of particle loss from L of 4.8 to 3.4 is the location of the pitch-angle instability reported by Williams et al. (1972) using the same instrumentation.

For the first storm the proton energy density for the 5-138 keV protons, which we have been considering, reached a maximum of 1.7×10^{-7} ergs/cm^3 at L=4.75 on Orbit 99, which at this L is an order of magnitude increase over the quiet time value. It also represents 93% of the total energy density in the 5-872 keV energy region. This maximum occurred in coincidence with a substorm seen at Leivogur from 0100 to 0200 U.T. on December 17, and simultaneous with a decrease in field strength as measured by the on-board magnetometer and a depression of field strength of the same form and duration as seen at San Juan (Cahill, 1972, Figure 4). This similarity in form between the two magnetometer records not only indicates that the bulk of the ring current was outside of the orbit of the satellite, but that the enhancement was temporal rather

than spatial. If it were spatial the ground magnetometer would have continued to observe a depression after the satellite had departed from the enhancement region.

Figure 5 shows the same energy density profiles as Figure 4, but for three orbits associated with the second storm. Orbit 101 began with the sudden commencement when the satellite was near perigee and represents the growth or development stage of the storm. This orbit shows a very large gradient between 3.5 and 4.0 R_E, in which the energy density increased from 1.5×10^{-8} ergs/cm^3 at L=3.5 to 2.0×10^{-7} ergs/cm^3 at L=3.75, and continued to increase to 5.2×10^{-7} ergs/cm^3 at L=4.1 for the 5-138 keV protons. Further analysis is required to determine whether this is primarily a spatial or temporal effect. The steep gradient on the inbound leg has moved inward to L=2.5 during the early recovery phase, which is the closest in that the storm-time ring current has ever been observed. The profile of these protons for Orbit 102, during the later recovery phase of this second magnetic storm, is quite symmetric. While the radial distribution during Orbit 103 could still be characterized as symmetric, it shows an increase in the inbound leg from L=5 to L=4.3, which in magnetic-local-time is between 2200h and midnight.

CONCLUSIONS

In an effort to summarize the contrasting development of the storm-time ring current during the two magnetic storms, we have drawn maps indicating the proton energy density spatial/temporal distributions

for the 5 to 138 keV protons for each of the seven orbits. In Figure 6 the S^3-A orbit in geomagnetic coordinates in the equatorial region is shown for Orbits 97 through 103, with the proton energy density regions estimated on the basis of the orbital profiles of protons shown in Figures 4 and 5.

The first storm was not characteristic of a single substorm nor a fully developed magnetic storm, but it was comprised of a sudden commencement, a positive phase, and multiple substorms producing a small depression in the magnetic field (Cahill, 1972; Figure 1).

Orbit 97: The quiet-time ring current, comprised primarily of protons with energies greater than those considered here, is symmetrically distributed around the earth. The low energy portion which is shown is also symmetric at least out to satellite apogee.

Orbit 98: The sudden commencement of the first magnetic storm occurred near apogee, nearly coincident with the small enhancement of protons beyond L=5 outbound.

Orbit 99: This orbit was asymmetric in the energy density distribution, with considerably more energy near midnight than in the evening hours.

Orbit 100: In contrast to the previous orbit, the energy became skewed toward dusk with a deeper penetration of the current distribution at dusk and a loss of protons near midnight.

The second magnetic storm was more classical in development, although, the growth phase of about two hours was quite short.

Orbit 101: The large asymmetry between outbound and inbound legs was due to the storm development.

Orbit 102: Apparent symmetry was already achieved. Whether diffusion into the symmetric distribution or a loss of particles account for the large decrease in density requires further analysis.

Orbit 103: While seemingly normal for this stage of the storm, these distributions are anomalous because of their slight increase in intensities over the previous orbit, while the magnetic deformation at the surface of the earth continued to recover.

In contrasting the energy density distributions for the two storms, the fully developed storm displayed three dominant features over the undeveloped storm:

1. the intensities were $2\frac{1}{2}$ times larger;
2. the depths of penetration were $\frac{1}{2}$ to 1 R_E lower;
3. the distributions became symmetric.

ACKNOWLEDGMENTS

We wish to express particular appreciation to Dr. T. A. Fritz for his efforts toward including the solid state proton detector in the experiment complement of S^3-A. The work of S. H. Way, J. F. McChesney, J. Richards and S. L. Jones, and several technicians in preparing the solid state proton detector and channel multiplier detector is greatly appreciated.

We wish to thank Christine Gloeckler and R. W. Janetzke for assistance in data analysis.

REFERENCES

Cahill, L. R., Jr., Magnetic storm inflation in the evening sector, Univ. of Minn. Preprint, July 1972 (submitted to J. Geophys. Res.).

Davis, L. R., and J. M. Williamson, Outer zone protons, Radiation Trapped in the Earth's Magnetic Field, ed. Billy M. McCormac, D. Reidel Pub. Co., Dordrecht-Holland, pp. 215-230, 1965.

Frank, L. A., On the extraterrestrial ring current during geomagnetic storms, J. Geophys. Res., 72, 3753-3768, 1967.

Longanecker, G. W., and R. A. Hoffman, S^3-A spacecraft and experiment description, GSFC Preprint X646-72- 240, July 1972, (submitted to J. Geophys. Res.).

Sugiura, Masahisa, The ring current, to be published, Proceedings of the Symposium on "Critical Problems of the Magnetosphere Physics", COSPAR, Madrid, Spain, May, 1972.

Williams D. J., T. A. Fritz, and A. Konradi, Observations of proton spectra ($1.0 \leq E_p \leq 300$ keV) and pitch angle distributions at the plasmapause, NOAA Technical Memorandum, ERL SEL-21, June 1972 (submitted to J. Geophys. Res.)

FIGURE CAPTIONS

Figure 1. Proton energy density radial profiles in the equatorial region for the three energy rangers indicated as well as the total energy density for the entire region. The gap in the middle, at apogee, is to indicate that the satellite is sitting at approximately the same L-value while moving in local time.

Figure 2. Proton energy density radial profiles as described in Figure 1 for Orbit 102, which was during the recovery phase of the second magnetic storm.

Figure 3. Proton energy density spectrums at L=4 on the outbound leg of the S^3-A orbit for quiet-time, Orbit 97, and at the main phase of the second magnetic storm, Orbit 101.

Figure 4. Radial profiles for protons in the energy range 5 to 138 keV for four orbits associated with the first magnetic storm.

Figure 5. Radial profiles for protons in the energy range 5 to 138 keV for three orbits associated with the second magnetic storm.

Figure 6. Maps indicating the 5 to 138 keV proton energy density spatial/temporal distributions for each of the seven S^3-A orbits during the two storms. The orbit is drawn in geomagnetic coordinates in the equatorial region, with observed proton energy density regions shown.

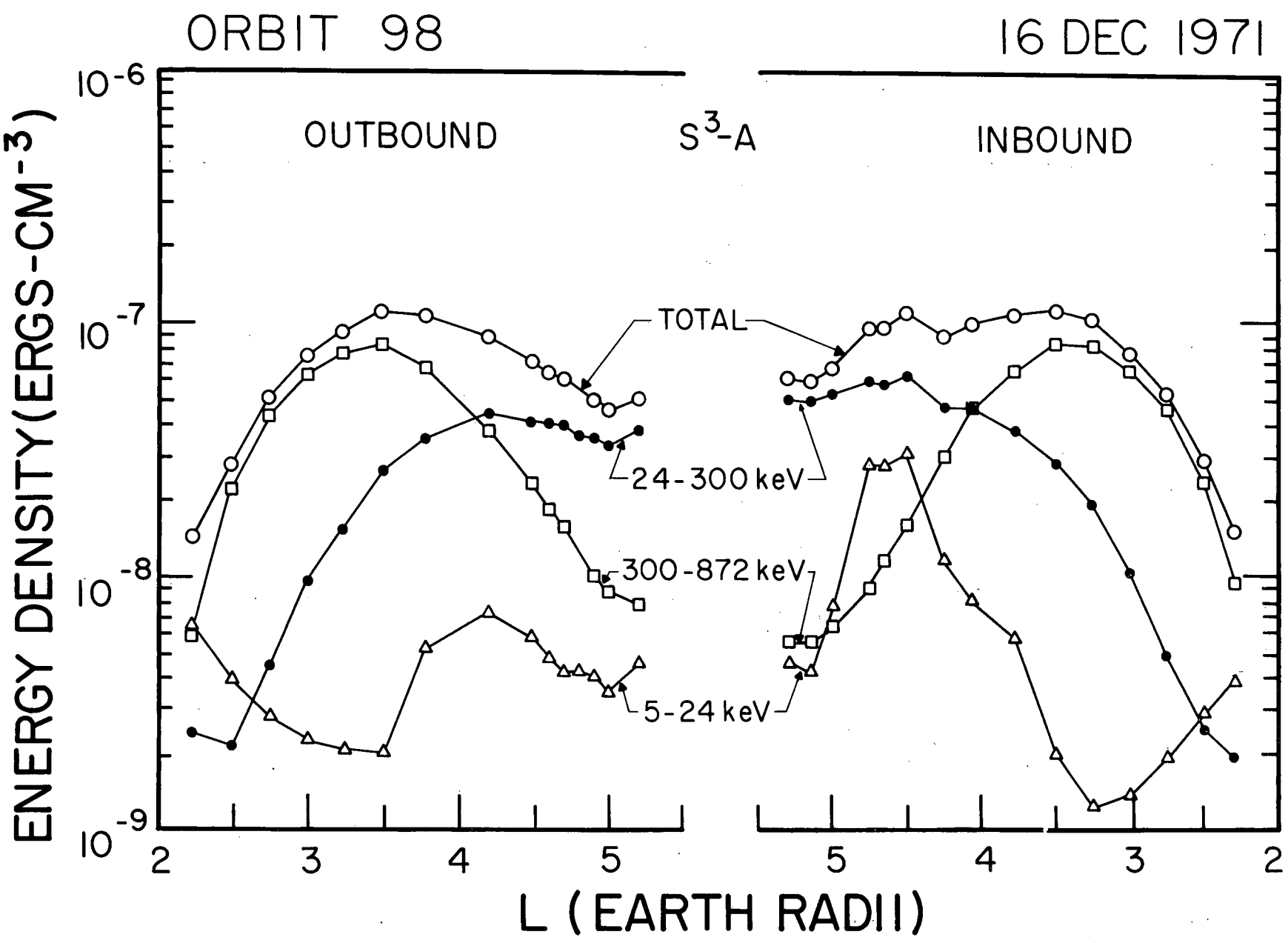
ORBIT 98
16 DEC 1971
OUTBOUND
S3-A
INBOUND
TOTAL
24-300 keV
300-872 keV
5-24 keV
ENERGY DENSITY(ERGS-CM-3)
10-6
10-7
10-8
10-9
2
3
4
5
L (EARTH RADII)

FIGURE 1

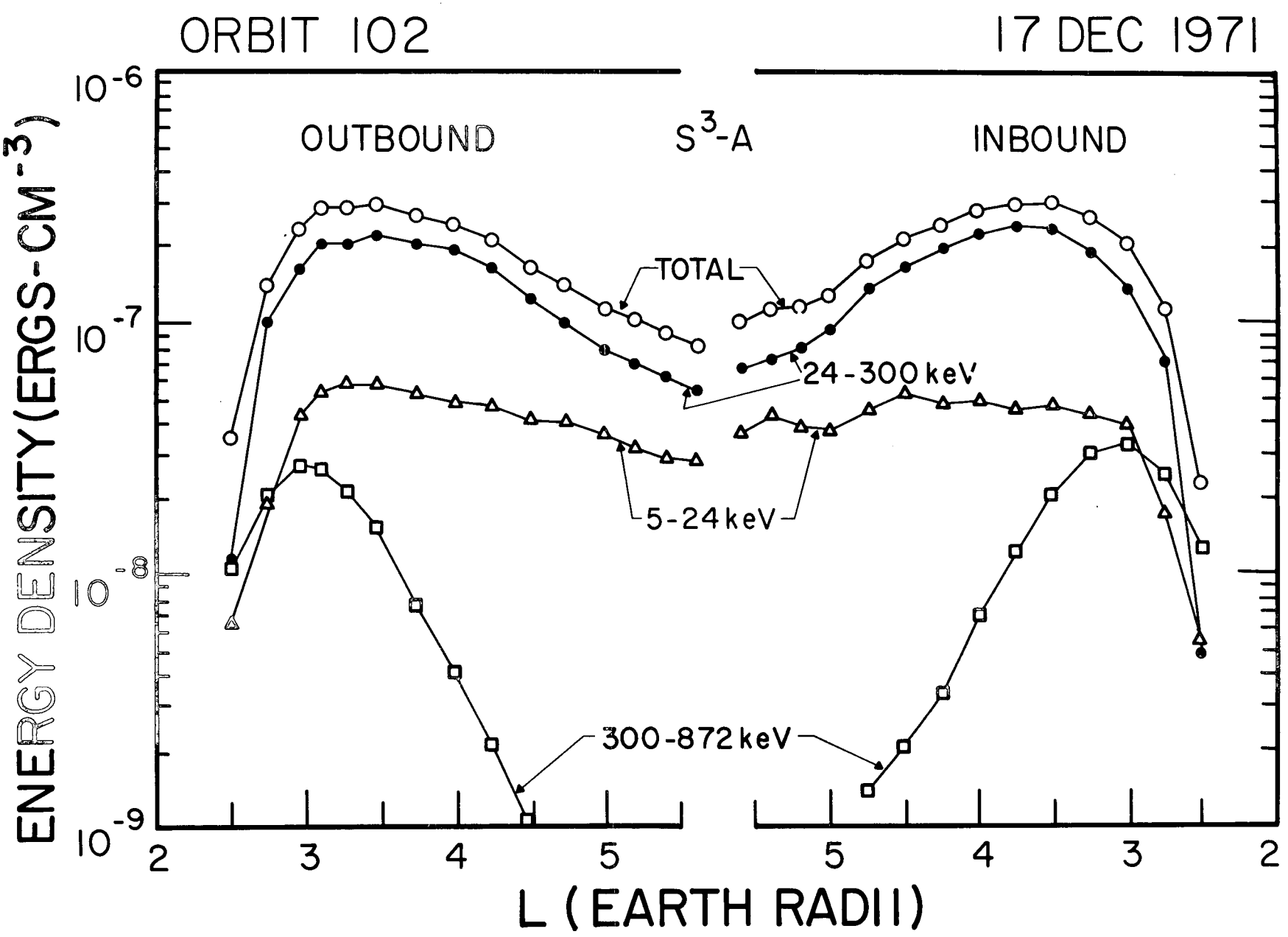
ORBIT 102
17 DEC 1971
OUTBOUND
S3-A
INBOUND
TOTAL
24-300 keV
5-24 keV
300-872 keV
ENERGY DENSITY (ERGS-CM-3)
10-6
10-7
10-8
10-9
2
3
4
5
5
4
3
2
L (EARTH RADII)

FIGURE 2

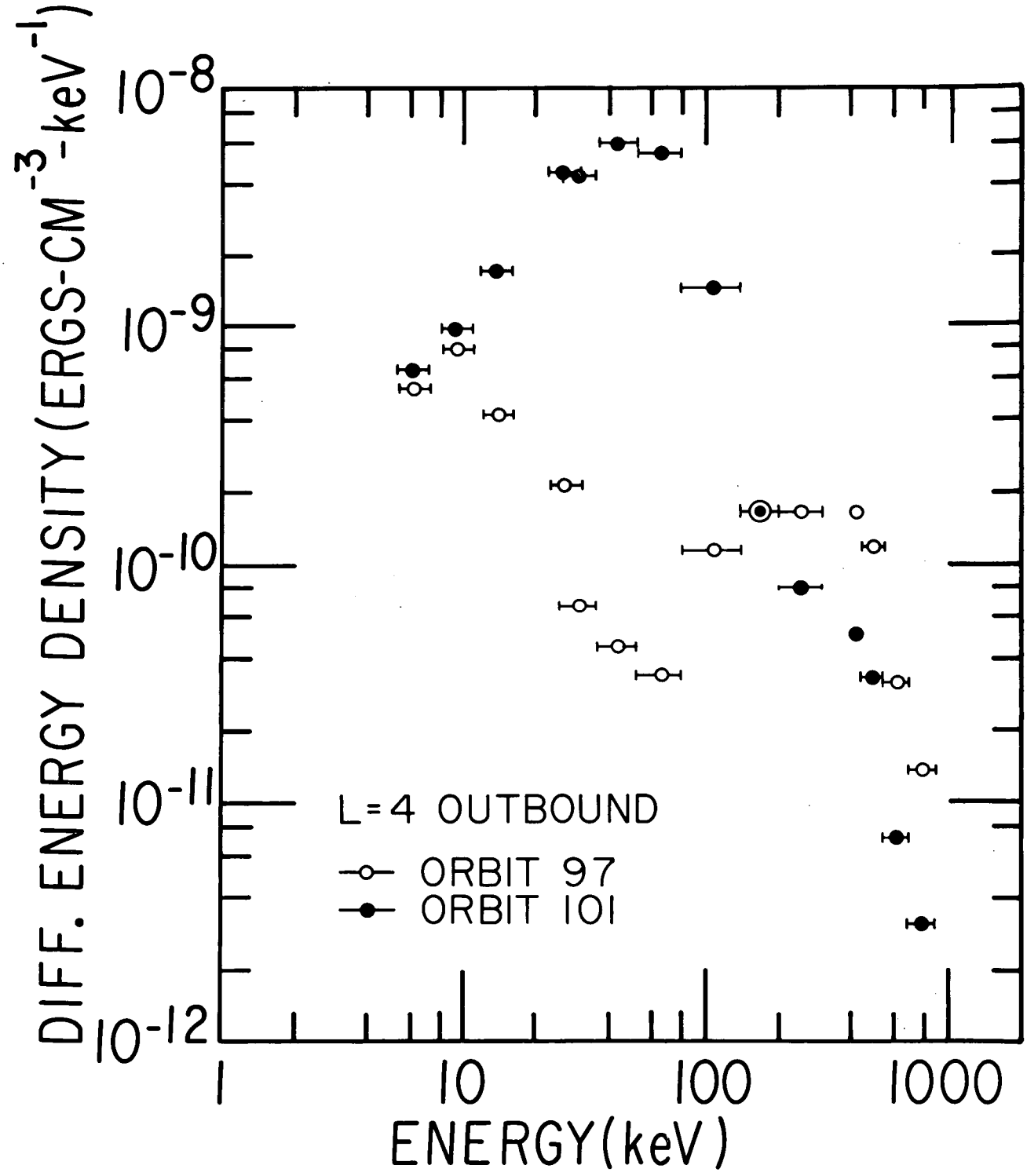
DIFF. ENERGY DENSITY (ERGS-CM^{-3}-keV^{-1})
10^{-8}
10^{-9}
10^{-10}
10^{-11}
10^{-12}
L=4 OUTBOUND
ORBIT 97
ORBIT 101
1
10
100
1000
ENERGY(keV)

FIGURE 3

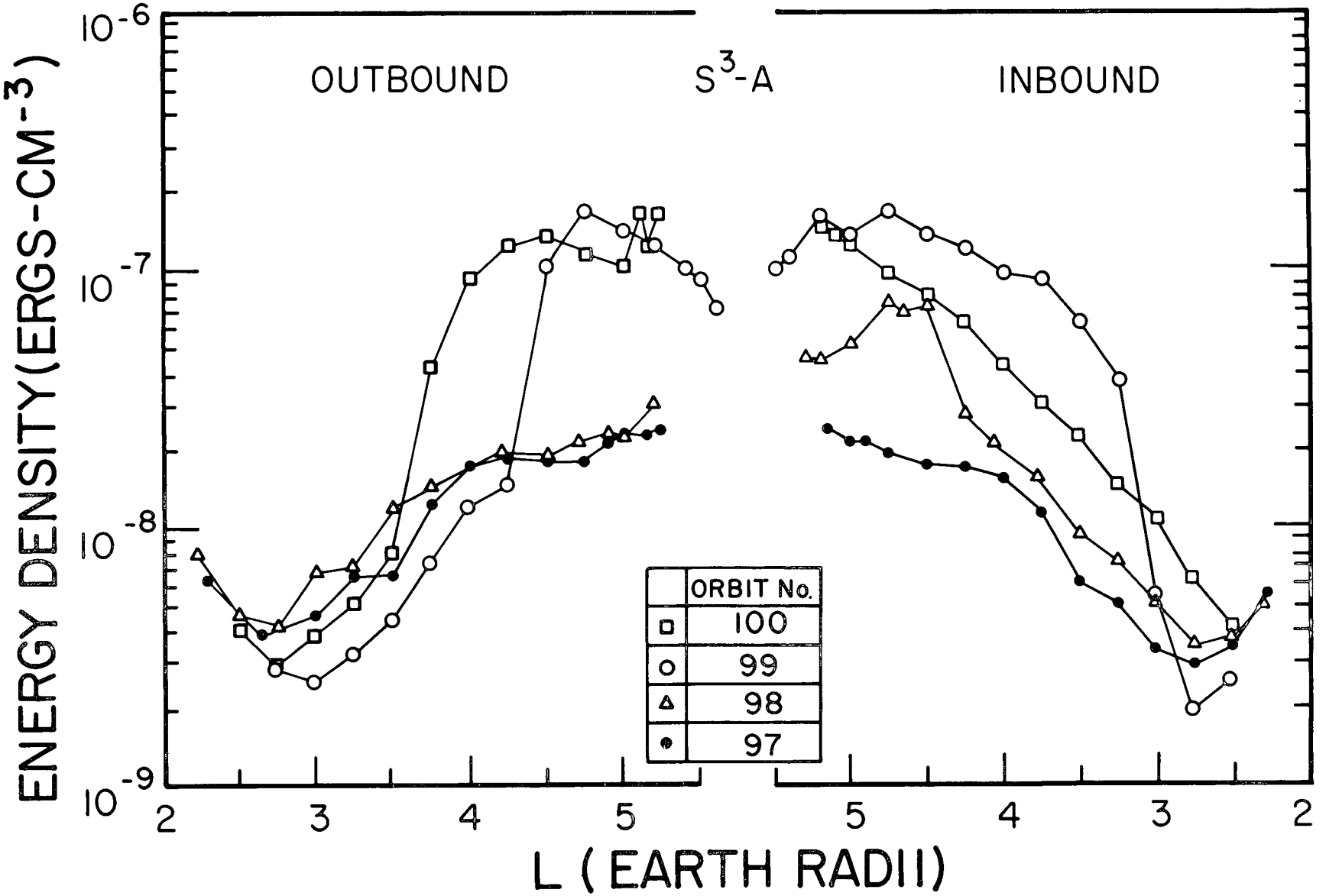
OUTBOUND
S3-A
INBOUND
ENERGY DENSITY(ERGS-CM-3)
10-6
10-7
10-8
10-9
2
3
4
5
5
4
3
2
L (EARTH RADII)
ORBIT No.
100
99
98
97

FIGURE 4

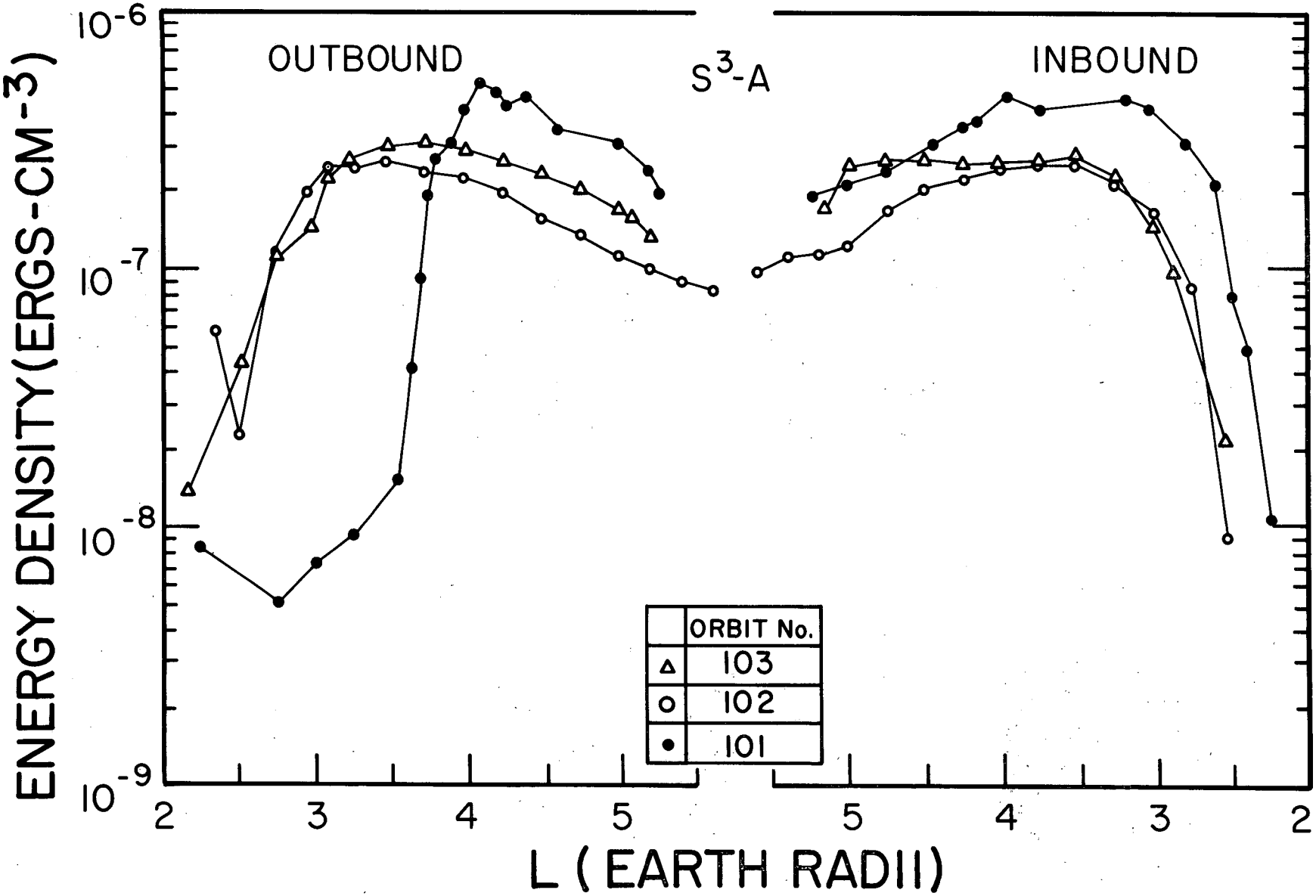
OUTBOUND
S3-A
INBOUND
ENERGY DENSITY(ERGS-CM-3)
10-6
10-7
10-8
10-9
2
3
4
5
5
4
3
2
L (EARTH RADII)
ORBIT No.
103
102
101

FIGURE 5

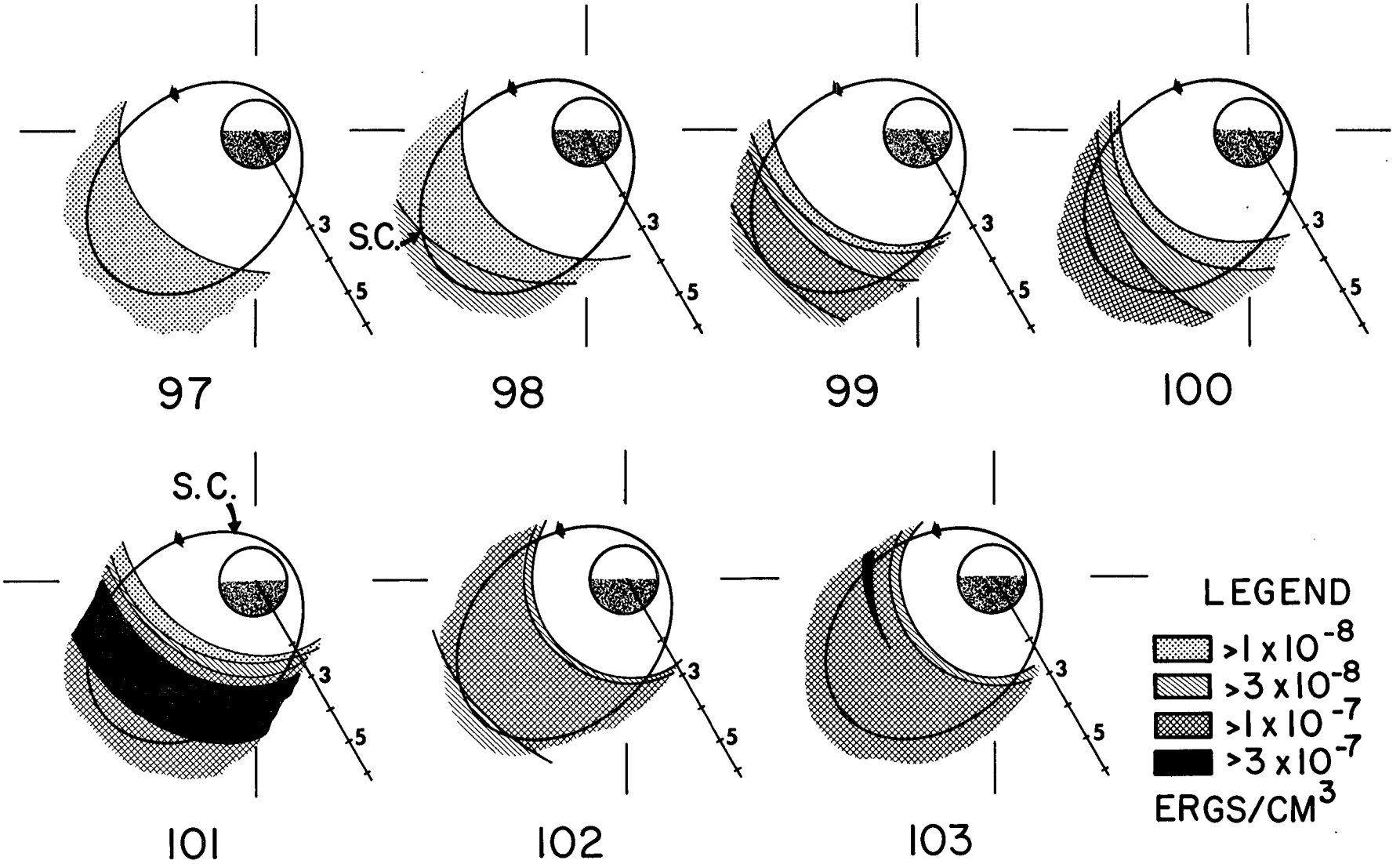
S.C.
3
5
97
98
99
100
S.C.
101
102
103
LEGEND
>1 x 10^-8
>3 x 10^-8
>1 x 10^-7
>3 x 10^-7
ERGS/CM^3

FIGURE 6